ImmunoHorizons
RESEARCH ARTICLE | NOVEMBER 30 2023

New Insights into the Complement Receptor of the Ig Superfamily Obtained from Structural and Functional Studies on Two Mutants

Huiquan Duan; ... et. al

Immunohorizons (2023) 7 (11): 806–818.
https://doi.org/10.4049/immunohorizons.2300064

ImmunoHorizons

RESEARCH ARTICLE

Innate Immunity

New Insights into the Complement Receptor of the Ig Superfamily Obtained from Structural and Functional Studies on Two Mutants

Huiquan Duan,* Troy G. Abram,* Ana Rita Cruz,† Suzan H. M. Rooijakkers,† and Brian V. Geisbrecht*

*Department of Biochemistry and Molecular Biophysics, Kansas State University; Manhattan, KS; and †Department of Medical Microbiology and Immunology, University Medical Center Utrecht, Utrecht, the Netherlands

ABSTRACT

The extracellular region of the complement receptor of the Ig superfamily (CRIg) binds to certain C3 cleavage products (C3b, iC3b, C3c) and inhibits the alternative pathway (AP) of complement. In this study, we provide further insight into the CRIg protein and describe two CRIg mutants that lack multiple lysine residues as a means of facilitating chemical modifications of the protein. Structural analyses confirmed preservation of the native CRIg architecture in both mutants. In contrast to earlier reports suggesting that CRIg binds to C3b with an affinity of ∼1 μM, we found that wild-type CRIg binds to C3b and iC3b with affinities <100 nM, but to C3c with an affinity closer to 1 μM. We observed this same trend for both lysine substitution mutants, albeit with an apparent ∼2- to 3-fold loss of affinity when compared with wild-type CRIg. Using flow cytometry, we confirmed binding to C3 fragment-opsonized *Staphylococcus aureus* cells by each mutant, again with an ∼2- to 3-fold decrease when compared with wild-type. Whereas wild-type CRIg inhibits AP-driven lysis of rabbit erythrocytes with an IC_{50} of 1.6 μM, we observed an ∼3-fold reduction in inhibition for both mutants. Interestingly, we found that amine-reactive crosslinking of the CRIg mutant containing only a single lysine results in a significant improvement in inhibitory potency across all concentrations examined when compared with the unmodified mutant, but in a manner sensitive to the length of the crosslinker. Collectively, our findings provide new insights into the CRIg protein and suggest an approach for engineering increasingly potent CRIg-based inhibitors of the AP. *ImmunoHorizons*, 2023, 7: 806–818.

INTRODUCTION

The extracellular complement system consists of dozens of soluble and cell surface–associated proteins and serves critical roles in many processes related to the innate immune response (1, 2). There are three canonical routes for initiation of complement activity known as the classical (CP), lectin (LP), and alternative (AP) pathways, which differ largely in the biochemical stimuli that trigger them. However, they all converge upon cleavage of the central complement component (i.e., C3) into its bioactive fragments (i.e., C3a and C3b) via two multisubunit proteases known as C3 convertases. The CP/LP C3 convertase (i.e., C4b2a) assembles following initiation of either the CP or LP. It consists of the activated form of the protease C2 bound

Received for publication August 25, 2023. Accepted for publication November 3, 2023.

Address correspondence and reprint requests to: Dr. Brian V. Geisbrecht, Kansas State University, 141 Chalmers Hall, 1711 Claflin Road, Manhattan, KS 66506. E-mail address: geisbrechtb@ksu.edu

ORCIDs: 0000-0003-3351-8618 (H.D.); 0000-0003-4102-0377 (S.H.M.R.); 0000-0002-1775-0727 (B.V.G.).

This work was supported by National Institutes of Health Grant R35GM140852 (to B.V.G.). Use of the Advanced Photon Source was supported by the U.S. Department of Energy, Office of Science, Office of Basic Energy Sciences Contract W-31-109-Eng-38.

The refined coordinates and structure factors presented in this article have been submitted to the RCSB Protein Data Bank under accession numbers 8TE5 and 8TE6.

Abbreviations used in this article: AP, alternative pathway; AS, active human serum; CP, classical pathway; CRIg, complement receptor of the Ig superfamily; CRIg-Mut-1, CRIg Ig V domain mutant K15R/K36R/K62R/K72R/K110R; CRIg-Mut-2, CRIg Ig V domain mutant K15R/K36R/K62Q/K72R/K110R; CRIg-WT, wild-type CRIg; HIS, heat-inactivated human serum; LP, lectin pathway; NHS, *N*-hydroxy-succinimide; PDB, Protein Data Bank; PEG, polyethylene glycol; SPR, surface plasmon resonance; RU, resonance unit; TCC, terminal complement complex.

The online version of this article contains supplemental material.

https://doi.org/10.4049/immunohorizons.2300064

in a Ca^{2+}-dependent complex to the platform molecule C4b. In contrast, the AP C3 convertase (i.e., C3bBb) assembles following initiation of the AP or in response to ongoing CP/LP activity. It consists of the activated form of the protease complement factor B bound in a Mg^{2+}-dependent complex to the platform molecule C3b. Because the AP C3 convertase generates the platform molecule upon which new convertases assemble, it serves as a powerful means of self-amplification, especially when localized to complement-reactive cells, surfaces, and materials.

One of the best understood aspects of complement function lies in the recognition, opsonization, and lysis of microorganisms, including bacteria (1, 2). In this setting, C3b deposition on bacterial cells promotes several effector mechanisms of complement. Increasing levels of cell surface C3b promotes association of a second copy of C3b with preformed C3 convertases and thereby changes their substrate preference toward cleavage and activation of C5 into C5a and C5b (3–6). Whereas formation of C5b triggers assembly of the terminal complement complex (TCC) (i.e., C5b–C9) that can directly lyse Gram-negative bacteria, the C5a generated serves as a potent chemoattractant to phagocytic cells. This latter effector mechanism is especially important in the case of Gram-positive bacteria (e.g., *Staphylococcus aureus*), which are resistant to attack by the TCC. Phagocytic cells typically express one or more classes of transmembrane complement receptors, which serve as selective ligands for the C3 fragments that serve as opsonins, namely C3b, iC3b, and C3d (1, 2, 7). These receptors facilitate the effector mechanism of opsonophagocytosis, whereby complement-opsonized bacteria are engulfed by phagocytes and subsequently killed within the phagosome by oxidative, proteolytic, or various other means (8).

The complement receptor of the Ig superfamily (CRIg) is expressed primarily by tissue-resident macrophages, whereby it promotes phagocytosis of C3-opsonized bacteria and particles (9, 10). Similar to other complement receptors, CRIg does not bind to native C3; however, it does bind to activated C3 fragments, including C3b, iC3b, and C3c (9, 11). The C3b-binding region of CRIg lies within its N-terminal Ig V domain (9) (Fig. 1A, 1B), which recognizes a discontinuous site within the so-called "key ring" core of C3 that is comprised primarily of its β-chain (11) (Fig. 1C, 1D). This binding site is unique from other complement receptors and regulators (7, 11, 12). Moreover, unlike other complement receptors (e.g., CR1) or regulatory proteins (e.g., complement factor H), CRIg lacks the canonical complement regulatory activities of accelerating decay of the AP C3 convertase or serving as a cofactor for complement factor I cleavage of C3b (11). The isolated C3b-binding domain of CRIg inhibits the AP, however, as it blocks activation of both C3 and C5 by their respective convertases (11). Further mechanistic studies showed that CRIg binding to C3b interferes with binding of C5 to the AP C5 convertase, but not to the CP/LP C5 convertase (11). These features make CRIg an intriguing template molecule for developing AP-selective inhibitors.

The last two decades have resulted in an increasingly sophisticated appreciation of the roles played by complement in either causing or promoting human inflammatory diseases (13, 14). This has led to a widespread interest in developing potent and specific inhibitors for therapeutic manipulation of the complement system (13, 14). The first Food and Drug Administration–approved complement-targeted therapeutic, eculizumab, is a humanized mAb that binds to an epitope accessible in native C5 and prevents its activation by C5 convertases (15, 16). CRIg likewise blocks C5 activation, albeit through the AP C5 convertase alone (11); however, CRIg has the additional activity of blocking upstream activation of C3 (11). Taking advantage of these properties, Katschke et al. (17) showed that a soluble form of murine CRIg blocked AP-driven inflammation in two different animal models of experimental arthritis. Subsequent work employed structure-based affinity maturation to enhance the potency of CRIg, as the affinity of this molecule for C3b was judged too weak (K_D = 1.1 μM) on its own to achieve full inhibition of the AP (18). Although a gain-of-function variant of CRIg was described (18), further development of CRIg for therapeutic purposes seems to have stalled.

In this study, we undertook a study with two objectives. First, we sought to provide more detailed information on CRIg binding to activated C3 fragments, including C3b, iC3b, and C3c. Our results show that CRIg binds to C3b and iC3b with affinities <100 nM, which is at least an order of magnitude tighter than originally reported. Second, we explored whether chemically crosslinked forms of CRIg could be prepared with enhanced inhibitory properties. To overcome heterogeneity resulting from amine-reactive crosslinking, we prepared two CRIg mutants where only a single lysine residue remained in the protein. We found that replacement of multiple lysine residues does not affect the overall structure of CRIg, and the two mutants exhibited only mild (i.e., <3-fold) loss of function when compared with wild-type. Interestingly, we observed enhanced AP inhibition using a chemically modified CRIg mutant when compared with the unmodified protein. Taken together, these results provide new insights into CRIg and suggest that modified forms of CRIg may be useful tools for basic studies of complement or for manipulating the AP therapeutically.

MATERIALS AND METHODS

Protein samples

Samples of C3b, iC3b, and C3c that had been purified from pooled human serum were obtained from Complement Technology. DNA fragments encoding wild-type and site-directed mutant forms of the CRIg Ig V domain (NCBI Reference Sequence NP_009199.1 residues 20–137) were synthesized individually and were subcloned into the prokaryotic expression vector pT7HMT (19). The corresponding plasmids were transformed into *Escherichia coli* BL21(DE3) cells. Cells were grown in 1 l of Terrific Broth (IBI Scientific) until an OD_{600} of 0.6–0.8 was reached, induced with 1 mM isopropyl β-D-thiogalactoside, and incubated at 37°C for an additional 16 h. Following harvest by centrifugation, the induced cells were resuspended and lysed

https://doi.org/10.4049/immunohorizons.2300064

using a solution of 100 mM Tris-HCl (pH 8.0), 10 mM imidazole, and 6 M guanidine HCl. After preparing a clarified extract via high-speed centrifugation, recombinant CRIg proteins were purified by Ni-NTA affinity chromatography under denaturing conditions using previously published methods (19, 20). Following elution, each purified protein was reduced with 1 mM Tris(2-carboxyethyl)phosphine at 37°C for 30 min, then dialyzed overnight against 2 l of 100 mM Tris-HCl (pH 8.6), 20 mM glycine, 2 mM L-cysteine, 0.5 mM EDTA, and 2.5 M urea. Each sample was then dialyzed overnight against 4 l of PBS (pH 7.4). When necessary, the affinity tag was digested using tobacco etch virus protease as previously described (19, 20). Briefly, tobacco etch virus was added to the target protein at a 100:1 mass ratio and incubated overnight at room temperature. The digested sample was reapplied to a Ni-NTA affinity column, and the unbound fraction was collected. Final purification was achieved by gel-filtration chromatography using a Superdex 75 26/60 column (Cytiva Life Sciences) with PBS (pH 7.4) as the running buffer. Fractions were analyzed by SDS-PAGE and those containing purified CRIg proteins were pooled, concentrated, quantitated, and stored at either 4°C or −80°C for later use.

Samples of CRIg-Mut-1 (CRIg Ig V domain mutant K15R/K36R/K62R/K72R/K110R) that had been crosslinked by reactive polyethylene glycol (PEG) derivatives were prepared by incubating CRIg-Mut-1 with a corresponding Bis-PEG-NHS (*N*-hydroxy-succinimide) ester. Purified CRIg-Mut-1 was concentrated to 10 mg/ml and incubated with 2-fold molar excess of Bis-PEG_{12}-NHS ester or Bis-PEG_{25}-NHS ester (BroadPharm) for 1 h at room temperature according to the manufacturer's suggestions. The reaction was terminated by gel-filtration chromatography using a Superdex 75 26/60 column (Cytiva Life Sciences) with PBS (pH 7.4) as the running buffer. The column eluate was analyzed by SDS-PAGE and fractions containing crosslinked CRIg-Mut-1 were pooled, concentrated, quantitated, and stored at either 4°C or −80°C for later use.

Crystallization, x-ray diffraction, structure solution, and refinement

Samples of CRIg-Mut-1 and CRIg-Mut-2 (CRIg Ig V domain mutant K15R/K36R/K62Q/K72R/K110R) were prepared at 10 mg/ml in double-distilled H_2O. Initial crystallization conditions were identified by vapor diffusion of sitting drops that were prepared by a Crystal Gryphon liquid handling system (Art Robbins Instruments) using the Crystal Screen HT and Index HT screening kits (Hampton Research). Individual crystals of each protein were prepared by vapor diffusion of hanging drops at 20°C that were established by mixing 1 μl of protein solution with 1 μl of precipitant solution consisting of 0.1 M sodium acetate (pH 6.5), 0.2 M ammonium acetate, and 30% (w/v) PEG-4000 and equilibrating over 500 μl of the same precipitant solution. Crystals were cryopreserved by a brief incubation in a buffer consisting of precipitant solution supplemented with 5% (v/v) PEG-400 followed by flash cooling in liquid N_2.

X-ray diffraction data were collected at beamline 22-ID of the Advanced Photon Source at Argonne National Laboratory. Diffraction data were processed using the HKL-2000 software package (21). Phaser was used to solved each structure by molecular replacement (22) with the reduced and scaled reflection file as an input and the structure of the wild-type CRIg (CRIg-WT) Ig V domain (Protein Data Bank [PDB] entry 2ICC) as a search model (11). Structure solutions were improved through a combination of automated and manual rebuilding and refined by reciprocal space positional and B-factor refinement implemented within the Phenix software suite (23, 24). The refined models of CRIg-Mut-1 and CRIg-Mut-2 have been deposited in the PDB using accession codes 8TE6 and 8TE5, respectively. Additional information on x-ray diffraction data collection statistics and the properties of each model can be found in Table I.

Surface plasmon resonance binding studies

Surface plasmon resonance (SPR) experiments were performed on a Biacore T200 instrument at 25°C using a flow rate of 30 μl/min and a running buffer of HEPES-buffered saline with Tween 20 (20 mM HEPES [pH 7.4], 140 mM NaCl, and 0.005% [v/v] Tween 20). A ligand capture strategy using NiD200M Ni^{2+} chelator-modified sensor chips (XanTec bioanalytics) was employed as follows. First, NiD200M surfaces were conditioned for 1 min with 350 mM EDTA (pH 8.0). Second, a solution of 0.5 mM nickel chloride was then injected for 1 min followed by a 1 min wash with 3 mM EDTA (pH 8.0). Third, His-tagged CRIg proteins were captured on individual experimental flow cells (i.e., fc2, fc3, and fc4) at densities between 1000 and 1600 resonance units (RU), and a single flow cell was reserved for reference subtraction (i.e., fc1); an additional set of experiments were performed with His-tagged CRIg-WT, where a lower density of 130–200 RU was captured. Finally, following surface stabilization by equilibration in running buffer, single cycle kinetic series were collected using five concentrations of C3b, iC3b, and C3c (i.e., 0.8, 4, 20, 100, and 500 nM). Kinetic evaluation was performed on each reference-subtracted injection series using either a 1:1 (Langmuir) or two-state binding model as implemented in the Biacore T200 evaluation software (Cytiva). Observed K_a, K_d, and apparent K_D were determined from the resulting fits and are presented as the mean ± SD from four technical replicates as shown in Table II.

Binding of CRIg proteins to C3-opsonized *S. aureus*

mAmetrine-labeled *S. aureus* Newman Δ*spa/sbi* cells were constructed as previously described (25). Bacteria were grown overnight in Todd–Hewitt broth plus 10 μg/ml chloramphenicol, diluted to an OD_{600} of 0.05 in fresh Todd–Hewitt broth plus chloramphenicol, and cultured until the midlog phase (OD_{600} of 0.5). Bacteria were then washed and resuspended in RPMI-H medium (RPMI 1640 + 0.05% [w/v] human serum albumin) and stored until use at −20°C. Newman Δ*spa/sbi* (7.5×10^5 CFU) were incubated with 3-fold serial dilutions (starting from 10% [v/v]) of active human serum (AS) or heat-inactivated

human serum (HIS), or with 3% (v/v) AS/HIS in RPMI-H. Unless stated otherwise, all incubation steps were performed under shaking conditions (700 rpm) for 30 min at 37°C, followed by a single wash with RPMI-H and separation by centrifugation (3600 rpm for 7 min). C3-opsonized bacteria were incubated with 25 μl of 5 μg/ml, or with a 3-fold dilution series (starting from 15 μg/ml) of His-tagged forms of CRIg-WT, CRIg-Mut-1, CRIg-Mut-2, or untagged CRIg-WT in RPMI-H. To detect CRIg, bacteria were incubated for 30 min at 4°C with shaking with a FITC-conjugated mouse anti-His tag Ab (clone AD1.1.10, LifeSpan BioSciences) that had been diluted 1:80 in RPMI-H. After a final wash with RPMI-H by centrifugation, samples were fixed with 1% (w/v) paraformaldehyde in RPMI-H, and the fluorescent signal was detected using flow cytometry (BD FACSVerse). Data were analyzed using FlowJo software.

Hemolysis assay

Assays that quantified AP-mediated lysis of rabbit erythrocytes were used to monitor the complement inhibitory properties of CRIg proteins. Briefly, all assays were conducted in a 100-μl reaction mixture consisting of 12 μl of AS (Creative Biolabs), 50 μl of 0.1% (w/v) gelatin veronal buffer (GVB^o without Mg^{2+} and Ca^{2+}; Complement Technologies), 10 μl of 0.1 M MgEGTA (Complement Technologies), 8 μl of each protein sample in GVB^o needed to achieve the indicated final concentration, and 20 μl of rabbit erythrocytes (5×10^8/ml exchanged into GVB^o) that were resuspended immediately prior to beginning each assay. After 30 min at 37°C, all samples were centrifuged for 10 min at 200 × *g* and the supernatant was collected. The supernatants were diluted 4-fold in water and the absorbance was determined at 412 nm. Percent inhibition was determined by the following equation: $100 - 100[(OD_{412,\ sample} - OD_{412,\ buffer})/(OD_{412,\ no\ inhibitor} - OD_{412,\ buffer})]$. Apparent IC_{50} values and associated confidence intervals were determined by a four-parameter fit using GraphPad Prism software.

Data availability

The refined coordinates and structure factors have been deposited in the RCSB PDB (http://wwpdb.org/) under accession numbers 8TE5 and 8TE6.

RESULTS

Design of lysine substitution mutants of CRIg

Human CRIg exists as two isoforms that are generated via alternative splicing of transcripts (9). The longer isoform is expressed as a preprotein of 399 aa and differs from the shorter isoform primarily by the presence of a C2-class Ig domain (Fig. 1A). The C3b-binding activity of CRIg arises from its N-terminal Ig V domain, however, which allows both the long and short isoforms to act as cell surface–retained complement receptors (9). The Ig V domain itself consists of 118 residues (~13.4 kDa) and adopts a canonical β-sandwich fold (11), where the N and C termini are located at opposite poles of the protein (Fig. 1B). Structures of this Ig V domain bound to human C3b (Fig. 1C) and C3c (data not shown) reveal a large and discontinuous binding interface between CRIg and its C3-derived ligands (11). The CRIg-binding site on C3b is comprised of macroglobulin-like 3–6 domains, as well as the so-called linker domain (LNK) of the C3b β-chain. Although this binding site is accessible in the structures of C3b (26), iC3b, (27) and C3c (28), it remains masked in native C3 owing to a slight rotation of the macroglobulin-like 3 domain relative to the remainder of the β-chain (28). The CRIg-binding site is also absent from C3d, as this fragment is proteolytically released from the remainder of the C3-derived polypeptide. Taken together, these features allow CRIg to bind selectively those forms of activated C3 that also contain a β-chain (Fig. 1D).

Primary amines, such as those found at the N terminus of polypeptides or on the sidechains of lysines, represent an abundant functional group of proteins. In that regard, the CRIg Ig V domain contains six lysine residues (K15, K36, K62, K72, K110, and K118) in addition to its N terminus (Fig. 1A, 1B). Aside from K118, which appears to form a distant salt bridge with the sidechain of E277 in C3b and C3c (11), only the sidechain of K62 appears to be significantly buried at the interface of C3b. Therefore, we hypothesized that it would be possible to prepare multi lysine-to-arginine substitution mutants in the CRIg Ig V domain. By mutating multiple lysine residues to arginine simultaneously, a reduced number of free amines would be present on the variants that result. Furthermore, with a limited number of primary amines present, those amines that remained could be used in protein chemistry approaches to generate crosslinked or otherwise modified forms of the protein that might have enhanced functional properties.

Subsequently, we designed two different multiple lysine-to-arginine substitution mutants in the CRIg Ig V domain. These mutants are hereafter referred to as CRIg-Mut-1 and CRIg-Mut-2. CRIg-Mut-1 consists of five simultaneous lysine-to-arginine substitutions, K15R/K36R/K62R/K72R/K110R, but retains the K118 as in the wild-type protein. CRIg-Mut-2 also retains K118, but consists of four lysine-to-arginine substitutions, K15R/K36R/K72R/K110R, as well as a K62Q mutation. This latter mutation was made to avoid unexpected loss of C3 fragment binding that might result from insertion of the comparatively large arginine sidechain at a potentially sensitive area of the protein–protein interface.

Structural analysis of lysine substitution mutants of CRIg

We expressed CRIg-Mut-1 and CRIg-Mut-2, as well as a wild-type control, as His-tagged fusion proteins in *E. coli* (Fig. 2A). Following purification of the recombinant proteins under denaturing conditions, we refolded each protein using a previously published procedure and characterized the renatured molecules (20) (see *Materials and Methods*). Using analytical scale gel-filtration chromatography, we found that the CRIg-Mut-1 and CRIg-Mut-2 eluted as a single species at an apparent molecular mass comparable to that of CRIg-WT but intermediate to that

https://doi.org/10.4049/immunohorizons.2300064

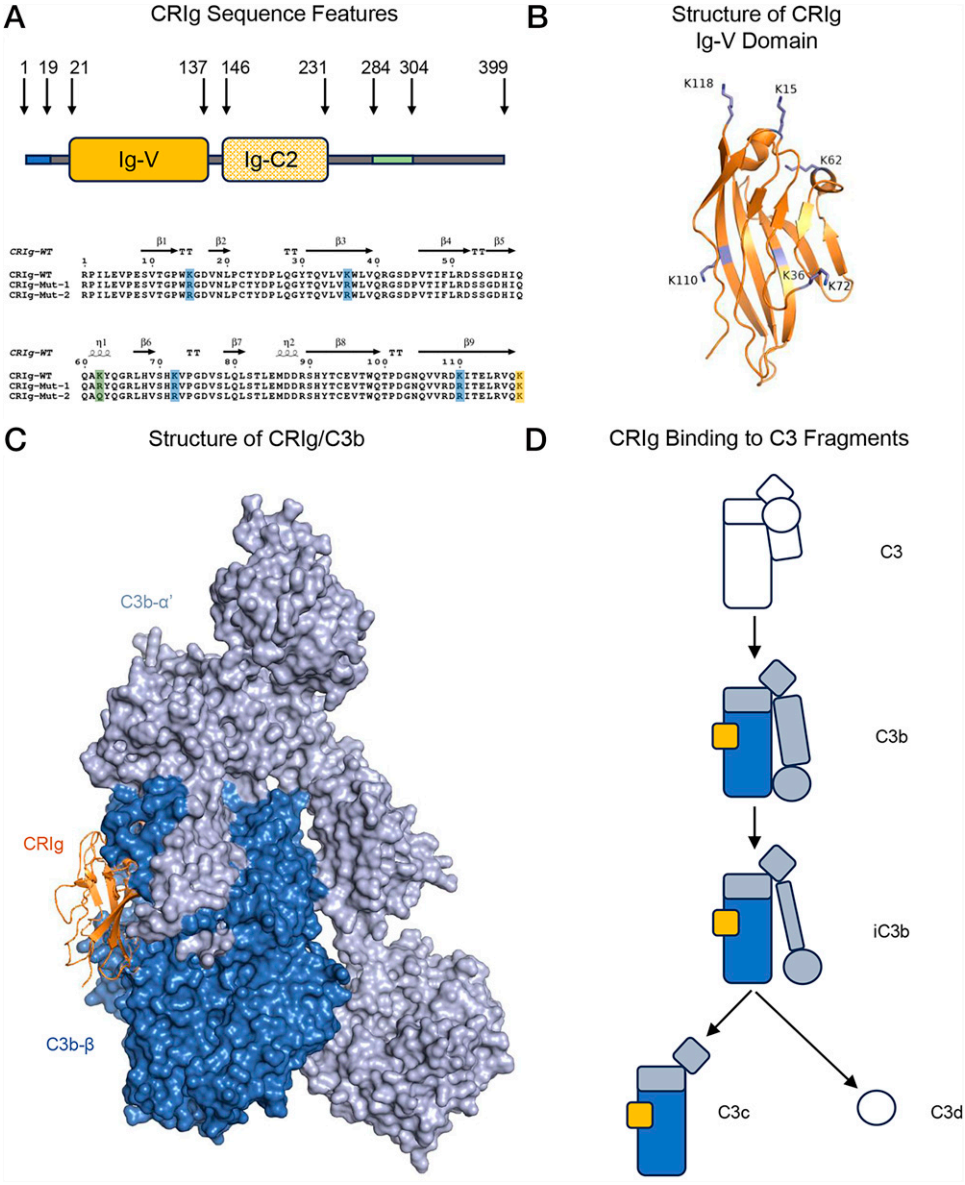

FIGURE 1. Sequence and structure features of the complement receptor of the Ig superfamily.

(**A**) Top, Schematic diagram of the complement receptor of the Ig superfamily (CRIg) preprotein is shown for its long isoform indicating the presence of the signal peptide (blue), Ig V (solid orange), Ig C2 (patterned orange), and transmembrane (green) domains. Amino acid positions defining approximate domain boundaries are numbered above the diagram. Bottom, Sequence comparison of the Ig V domains for CRIg-WT, CRIg-Mut-1, and CRIg-Mut-2 is shown along with the secondary structure elements seen in the crystal structure of CRIg-WT (11). The positions of lysines mutated to arginines in both CRIg-Mut-1 and CRIg-Mut-2 are highlighted in blue, and the lysine mutated to either arginine or glutamine is highlighted in green. The C-terminal lysine is highlighted in orange. (**B**) Depiction of the CRIg Ig V domain (orange ribbon) with its lysine residues in blue. The structure is drawn from PDB entry 2ICC (11). (**C**) Depiction of the CRIg Ig V domain (orange ribbon) bound to C3b (molecular surface), where its β-chain is dark blue and its α′-chain is light blue. The structure is drawn from PDB entry 2ICF (11). (**D**) Schematic representing CRIg (orange rectangle) binding to various forms of C3. C3 fragments that CRIg does not bind are depicted as hollow shapes, and those that it does bind are depicted in solid colors. The C3 β-chain is drawn in dark blue, and the α′-chain is drawn in light blue for CRIg-binding fragments of C3.

of BSA (66 kDa) and chicken lysozyme (14.3 kDa) (Fig. 2B). To gain further insight into the structural properties of these proteins, we crystallized both mutants and determined their structures by X-ray diffraction methods (Table I). We solved the structure of CRIg-Mut-1 to 1.25 Å limiting resolution and refined the model to R_{work} and R_{free} values of 16.4 and 19.6%, and we solved the structure of CRIg-Mut-2 to 1.5 Å limiting resolution and refined the model to R_{work} and R_{free} values of 16.6 and 22.3%. We found that CRIg-Mut-1 and CRIg-Mut-2 adopted structures essentially identical to CRIg-WT (Fig. 2C,

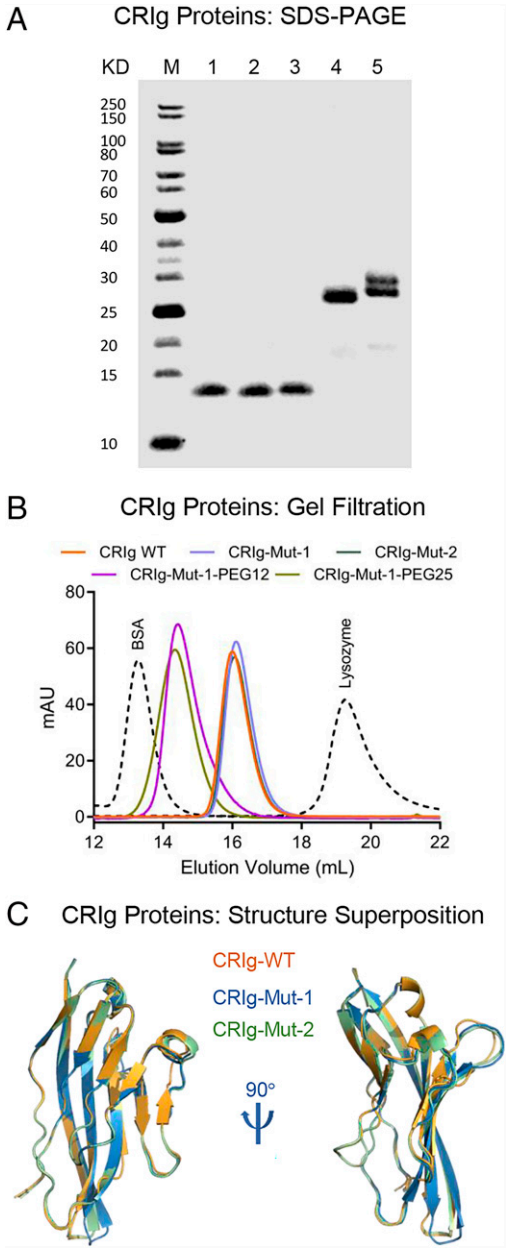

FIGURE 2. Physical characterization of lysine substitution mutants of CRIg.

(**A**) Samples of recombinant CRIg proteins and their cross-linked derivatives were processed under nonreducing conditions, separated by SDS-PAGE, and visualized by Coomassie Blue staining. Lane M, molecular mass marker; lane 1, CRIg-WT; lane 2, CRIg-Mut-1; lane 3, CRIg-Mut-2; lane 4, CRIg-Mut-1-PEG_{12}; lane 5, CRIg-Mut-1-PEG_{25}. (**B**) Samples of recombinant CRIg proteins and their cross-linked derivatives were separated by analytical size-exclusion chromatography. A legend identifying the chromatograms corresponding to individual proteins is inset. Chromatograms corresponding to the control proteins BSA and lysozyme are shown as a dashed line. (**C**) Comparison of the x-ray crystal structures for CRIg-WT, CRIg-Mut-1, and CRIg-Mut-2. The final models of each polypeptide were superimposed and are represented as ribbon diagrams from two orthogonal views. A legend identifying each model and the axis of rotation is inset.

Supplemental Fig. 1), as the final models superimpose upon that of the wild-type protein with root mean square deviation values of 0.175 and 0.200 Å, respectively. These observations were consistent with our earlier observations using gel-filtration chromatography, and together they confirmed that both CRIg-Mut-1 and CRIg-Mut-2 were well-folded proteins even though each contained multiple site-directed mutations.

Interactions of lysine substitution CRIg proteins with C3 activation products

Previous studies have suggested that CRIg-WT binds C3b and C3c with comparable affinity and that the affinity of the CRIg extracellular domain for C3b is on the order of ~1 μM (9, 11, 18). However, most of these studies made use of dimeric ligands or receptors (e.g., Fc fusion proteins) that may have influenced somewhat the results obtained. To investigate this issue using an alternative approach, as well as to gain insight into the functional properties of CRIg-Mut-1 and CRIg-Mut-2, we used SPR to characterize the interaction of surface-bound CRIg proteins with various C3 fragments. We devised a ligand capture strategy where a His-tagged CRIg protein was captured on all three experimental flow cells of a Ni^{2+}-loaded biosensor surface followed by assessment of C3 fragment binding through single-cycle kinetics (Fig. 3A–C). We then performed each experimental series in quadruplicate to enable statistical evaluation of the reproducibility of our observations (Fig. 3D, Supplemental Figs. 2, 3, Table II).

We first measured binding of immobilized CRIg-WT, CRIg-Mut-1, and CRIg-Mut-2 to C3b (Fig. 3A–C, left panels) using surfaces of an intermediate ligand capture density between 1000 and 1600 RU of His-tagged protein. In these experiments, we found that CRIg-WT binds C3b with low nanomolar affinity (apparent K_D = 7.3 ± 0.2 nM), which is nearly 100-fold tighter than what has been reported previously (K_D = ~1 μM) (11, 18). Although we found that both CRIg-Mut-1 and CRIg-Mut-2 have lower affinities for C3b than the wild-type protein (apparent K_D = 25.2 ± 5.1 and 16.2 ± 0.5 nM, respectively), these values remain in the low nanomolar range. We next measured binding of immobilized CRIg proteins to iC3b using a similar approach (Fig. 3A–C, center panels). We determined that the interaction with iC3b was not well fit by a simple one-to-one model, but instead required a two-state model to describe the experimental data (Supplemental Fig. 2). Nevertheless, we found that CRIg-WT binds to iC3b with an affinity that is ~10-fold diminished when compared with C3b under these conditions (apparent K_D = 68.0 ± 9.2 nM). This result was surprising, considering that the CUB domain that is cleaved during generation of iC3b from C3b is far removed from the CRIg-binding site (Fig. 1C) (7, 11). As was the case for C3b, we also found that both CRIg-Mut-1 and CRIg-Mut-2 have lower affinities for iC3b than CRIg-WT (apparent K_D = 115 ± 23.2 and 84.6 ± 12.3 nM, respectively). Finally, we measured binding of the same three immobilized proteins to C3c using a similar approach (Fig. 3A–C, right panels). As with iC3b, the interaction with

https://doi.org/10.4049/immunohorizons.2300064

TABLE I. X-ray diffraction data, structure solution, and refinement statistics

	CRIg-Mut-1	CRIg-Mut-2
PDB accession code	8TE6	8TE5
Data collection		
Space group	$P2_12_12_1$	$P2_12_12_1$
Wavelength (Å)	1.000	1.000
Cell dimensions (a, b, c) (Å)	31.83, 50.28, 60.98	31.01, 49.78, 60.03
Resolution (Å)	50.00–1.25	50.00–1.50
Wilson B factor (Å^2)	13.9	22.6
Completeness (%)	94.0 (90.5)	99.1 (99.5)
$I/\sigma I$	12.3 (7.2)	8.9 (3.0)
R_{pim}	0.039 (0.129)	0.061 (0.376)
$CC_{1/2}$	0.986 (0.946)	0.996 (0.702)
Redundancy	7.8 (7.8)	7.0 (5.4)
Refinement		
Resolution (Å)	30.49–1.25	30.02–1.50
No. of reflections	25,744	14,849
R_{work}/R_{free} (%)	16.4/19.6	16.6/22.3
Atoms modeled		
Total	1114	1062
Amino acid atoms	962	960
Water	152	102
Ramachandran plot		
Favored/allowed (%)	94.02/5.98	94.02/5.98
Average B factors (Å^2)	20.2	30.4
Root mean square deviations		
Bond lengths (Å)	0.004	0.005
Bond angles (°)	0.79	0.80

Values in parentheses are for the highest-resolution shell. $CC_{1/2}$, correlation coefficient between intensity estimates from half datasets.

C3c also required a two-state model to describe the experimental data (Supplemental Fig. 2). Interestingly, we found that CRIg-WT binds to C3c with an affinity similar to the value that has been previously reported (apparent K_D = 623 ± 4.1 nM) (11, 18). We also noted that both CRIg-Mut-1 (apparent K_D = 2780 ± 971 nM) and CRIg-Mut-2 (apparent K_D = 1130 ± 193 nM) bind C3c weaker than CRIg-WT. Considering these observations as a whole, both CRIg-Mut-1 and CRIg-Mut-2 display diminished binding of ∼3- and 1.7-fold, respectively, when compared with CRIg-WT across all three C3 activation products we examined in this study (Fig. 3D, Supplemental Fig. 3, Table II).

We also remeasured the binding of immobilized CRIg-WT to the same C3 activation fragments using surfaces of lower ligand capture density between 130 and 200 RU of His-tagged protein (Supplemental Fig. 3, Table II). In these experiments, we observed a somewhat weaker affinity for C3b (apparent K_D = 47.2 ± 6.5 nM) but an enhanced affinity for iC3b (apparent K_D = 10.5 ± 4.3 nM). However, we found an affinity for C3c consistent with the value that we determined earlier using the higher density surface (apparent K_D = 598 ± 148 nM). Although the reasons for the observed differences in affinity of CRIg-WT for C3b and iC3b between these two surface densities are not clear, these two sets of experiments together strongly suggest that the affinity of CRIg-WT for C3b and iC3b is at least an order of magnitude greater than it is for C3c.

Lysine substitution CRIg proteins retain binding to C3-opsonized *S. aureus*

CRIg was originally characterized as a previously unknown receptor for C3 activation products expressed by various subsets of tissue-resident macrophages (9, 10). This work established a role for CRIg in phagocytic clearance of C3 fragment–opsonized materials. We therefore used a flow cytometry approach to compare the ability of CRIg-WT, CRIg-Mut-1, and CRIg-Mut-2 to recognize C3 fragment–opsonized particles (Fig. 4, Supplemental Fig. 4). In these experiments, *S. aureus* cells that are devoid of the two Ig-binding proteins Spa and Sbi (Newman Δspa/sbi) were incubated with various concentrations of AS or HIS as a control, probed with His-tagged forms of CRIg, and quantified by staining using a fluorescent anti–His tag Ab. When we incubated *S. aureus* cells with a dilution series of AS followed by probing with a fixed concentration of His-tagged CRIg-WT, we observed a dose-dependent increase in fluorescence (Fig. 4A, Supplemental Fig. 4). This signal was abolished when either untagged CRIg-WT was used as a probe or when HIS was used as a source of complement components. When the initial experiment was performed with either His-tagged CRIg-Mut-1 or CRIg-Mut-2, we observed a dose-dependent increase in fluorescence but with roughly half the signal intensity seen for CRIg-WT. Thereafter, we performed a titration study wherein we incubated *S. aureus* cells with a fixed concentration of AS, probed with increasing concentrations of His-tagged CRIg proteins, and stained using a fluorescent

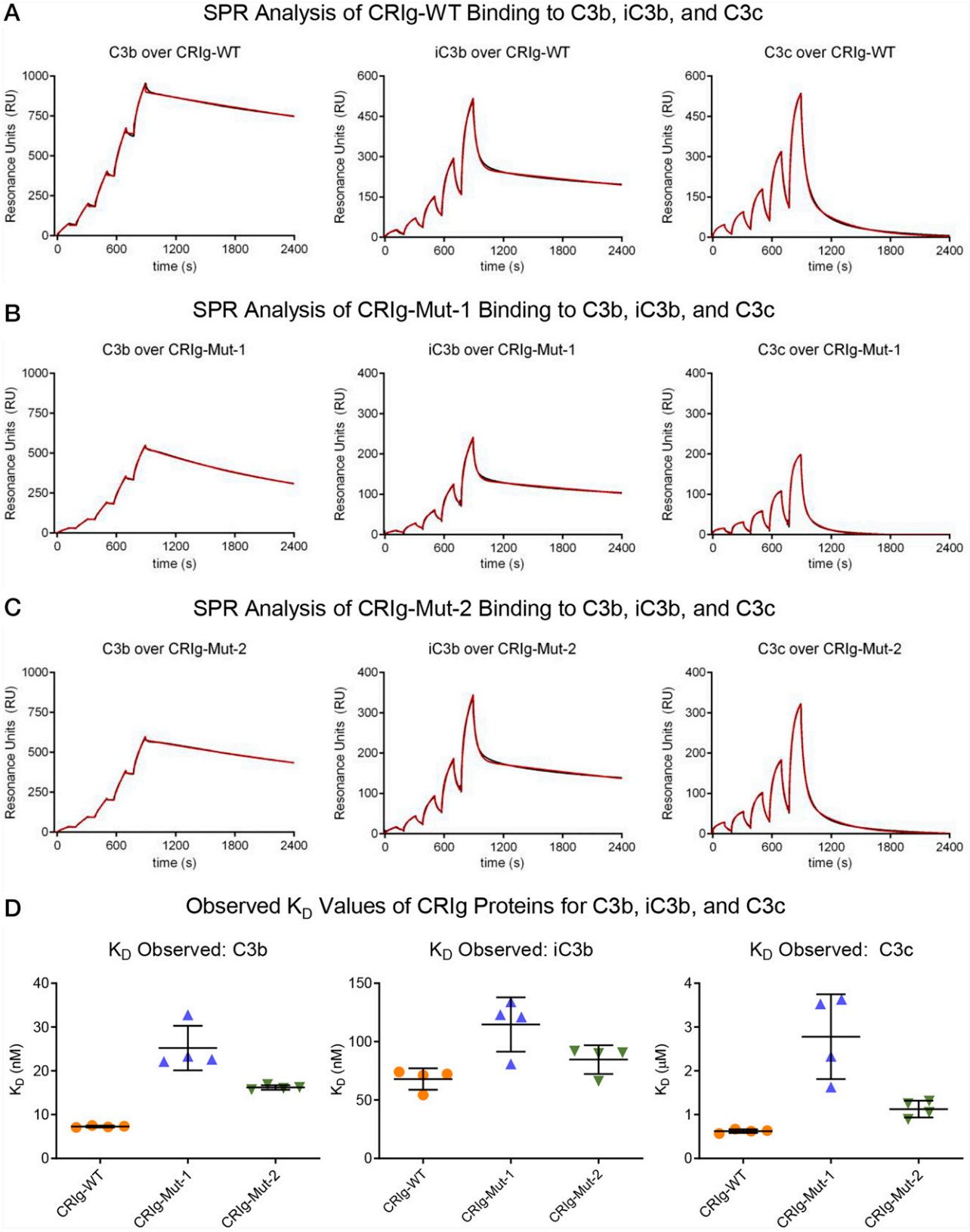

FIGURE 3. Direct binding studies of lysine substitution mutants of CRIg with various C3 activation fragments.

His-tagged forms of CRIg proteins were captured on three experimental flow cells of a Ni^{2+}-loaded biosensor while leaving one flow cell unmodified for reference subtraction. Protein–protein interactions were then monitored by injecting increasing concentrations of C3 activation ***(Continued)***

https://doi.org/10.4049/immunohorizons.2300064

TABLE II. Interaction parameters of C3 fragments with immobilized CRIg proteins

Analyte	Ligand	$K_{a\text{-}1}$ (10^4 M^{-1} s^{-1})	$K_{d\text{-}1}$ (10^{-4} s^{-1})	$K_{a\text{-}2}$ (10^{-3} s^{-1})	$K_{d\text{-}2}$ (10^{-4} s^{-1})	K_D (nM)	R_{max} (RU)
C3b	CRIg-WT[a]	1.71±0.03	1.25±0.03	—	—	7.29±0.20	1070±26
	CRIg-Mut-1[a]	1.82±0.50	4.41±0.58	—	—	25.2±5.07	721±47
	CRIg-Mut-2[a]	1.26±0.89	2.03±0.12	—	—	16.2±0.50	878±58
	CRIg-WT (LD)[b]	2.51±0.05	71.4±3.9	1.66±0.04	53.31±0.49	47.2±6.5	205±42
iC3b	CRIg-WT[b]	1.60±0.25	207±8.2	3.76±0.15	2.06±0.05	68.0±9.20	1260±94
	CRIg-Mut-1[b]	0.71±0.14	209±4.5	5.89±0.20	2.31±0.09	115±23.2	955±144
	CRIg-Mut-2[b]	1.06±0.17	191±2.0	4.69±0.13	2.27±0.05	84.6±12.3	979±82
	CRIg-WT (LD)[b]	3.58±0.28	168±7.0	4.63±0.22	1.05±0.40	10.5±4.3	148±35
C3c	CRIg-WT[b]	2.07±0.07	217±13	2.01±0.15	29.4±2.26	623±4.1	1380±88
	CRIg-Mut-1[b]	1.20±0.24	491±89	5.20±1.43	92.8±24.4	2780±971	1356±410
	CRIg-Mut-2[b]	1.48±0.09	271±34	2.62±0.51	41.4±7.95	1130±193	1160±160
	CRIg-WT (LD)[b]	2.58±1.78	288±162	0.37±0.03	3.88±1.45	598±148	873±67

All values are presented as the mean ± SD obtained for four replicate injections over the biosensor surface, except for the low-density surface, which used three replicate injections.
[a]Model accounts for a single binding site between the analyte and ligand described by one association and dissociation rate constant.
[b]Model accounts for a single binding site between the analyte and the ligand described by two sets of association and dissociation rate constants that are linked to one another.
LD, low density.

anti–His tag Ab. When we performed this experiment and probed with an increasing concentration of His-tagged CRIg-WT, we observed a dose-dependent increase in fluorescence as before (Fig. 4B, Supplemental Fig. 4). This signal was abolished when either untagged protein was used as a probe or when HIS was employed. However, when the titration experiment was performed with either His-tagged CRIg-Mut-1 or CRIg-Mut-2, we again observed a dose-dependent increase in fluorescence that was approximately half the intensity of CRIg-WT. Thus, the mild loss of function (~2- to 3-fold) seen for CRIg-Mut-1 and CRIg-Mut-2 in the SPR studies was also observed in cytometry experiments using C3 fragment–opsonized bacteria.

Inhibition of complement-mediated hemolysis by lysine substitution CRIg mutants

Although CRIg acts as a cell surface receptor of C3b/iC3b–opsonized materials (9, 10), its Ig V domain in isolation also inhibits the AP of complement by virtue of its interaction with C3b (11, 18). Previous work has revealed that CRIg binding to C3b blocks an important substrate binding site of the AP C3 and C5 convertases (of which C3b is an integral part), as CRIg appears to inhibit binding and cleavage of C3 and C5 by these convertases (11). Under normal physiological circumstances, assembly of the TCC requires proteolytic cleavage of C5 regardless of the initiation mechanism. Thus, any molecules that interfere with C5 cleavage will block TCC formation and inhibit complement-dependent lysis of erythryocytes. We therefore measured the efficiency of complement-driven lysis of rabbit erythrocytes in the presence of increasing concentrations of CRIg proteins under AP-specific conditions using AS as a source of complement components. We found that CRIg-WT inhibits hemolysis (IC_{50} = 1.6 μM) more potently than either CRIg-Mut-1 (IC_{50} = 4.9 μM) or CRIg-Mut-2 (IC_{50} = 5.0 μM) (Fig. 5A). Nevertheless, the relative change in IC_{50} we observed between these proteins is comparable to that we found previously in both the SPR (Fig. 3, Table II) and cytometry studies (Fig. 4). Note that although the observed IC_{50} values are considerably higher than the apparent K_D values observed by SPR (Table II), they are consistent with the expected C3b levels present under these assay conditions (i.e., 12% [v/v] AS is ~0.78 μM C3).

Our previous experiment showed that CRIg-Mut-1 displays an ~3-fold decrease in AP inhibition when compared with CRIg-WT. However, this relatively small loss of function suggested that CRIg-Mut-1 might still be amenable for further study including chemical modifications that enhance its activity. Because linking of functional units into a single species can contribute to increased activity through avidity-like effects, we wondered whether the same might also be possible for CRIg-Mut-1. CRIg-Mut-1 has only a single lysine residue (i.e., K118) in addition to its N terminus, and so we predicted that reaction of this protein with bifunctional, amine-reactive crosslinkers could be used to generate relatively homogeneous species for functional studies. Bis-PEG-NHS esters are symmetric, water-soluble derivatization reagents that react with primary amines and are available in various chain lengths. Therefore, we modified CRIg-Mut-1 with either a Bis-PEG_{12}-NHS ester or a Bis-PEG_{25}-NHS ester and purified the crosslinked species via size-exclusion chromatography (Fig. 2A). The expected molecular masses of CRIg-Mut-1-PEG_{12} and CRIg-Mut-1-PEG_{25} are 27.6 and 28.2 kDa, respectively, which corresponds well to the behavior of both molecules in size-exclusion chromatography and nonreducing SDS-PAGE experiments (Fig. 2A, 2B). Thus,

fragments in single-cycle mode. Sensorgrams were analyzed using standard procedures (see *Materials and Methods*). (**A**) Binding of C3b, iC3b, and C3c to CRIg-WT. (**B**) Binding of C3b, iC3b, and C3c to CRIg-Mut-1. (**C**) Binding of C3b, iC3b, and C3c to CRIg-Mut-2. (**D**) Comparison of the apparent K_D values from four replicate injections of C3b, iC3b, and C3c across all three forms of CRIg. Note the roughly 10-fold differences in affinity between C3b, iC3b, and C3c observed independently of the CRIg protein on the surface.

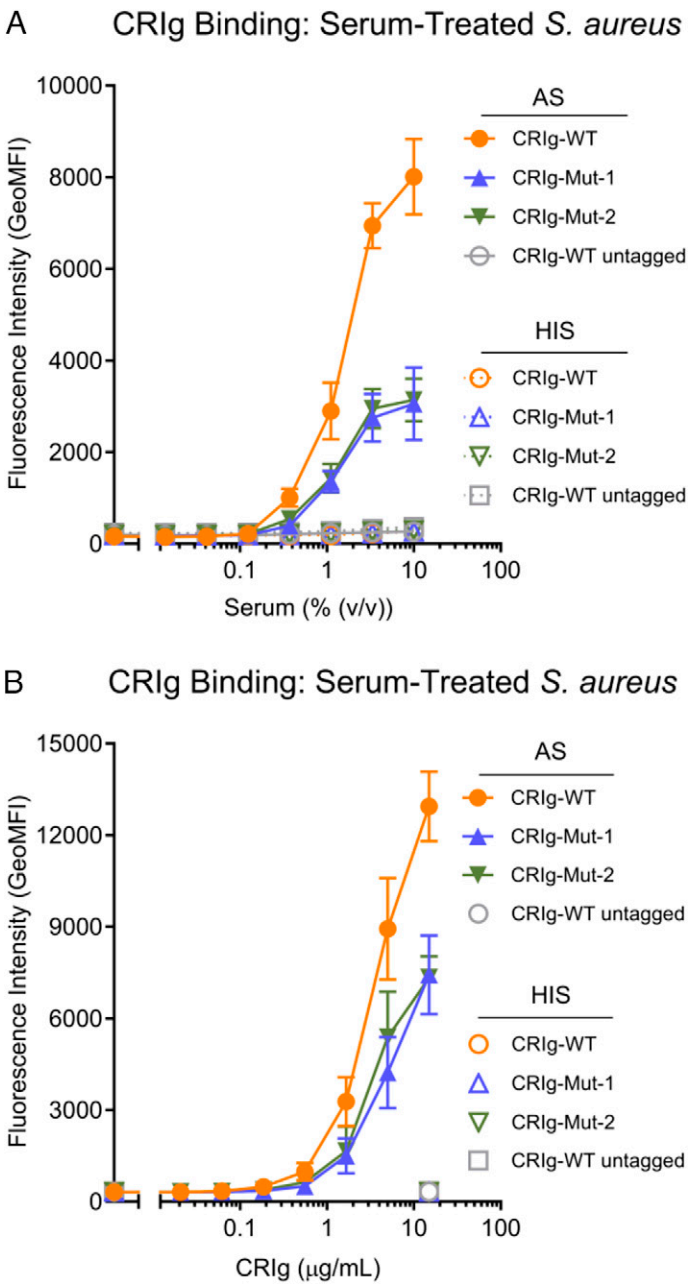

FIGURE 4. Assessment of binding to C3-opsonized *S. aureus* cells by lysine substitution CRIg mutants.

Cells of an *S. aureus* strain lacking Ig-binding activity were incubated with either active human serum (AS) or heat-inactivated human serum (HIS). CRIg binding was assessed by flow cytometry following incubation of various samples with His-tagged CRIg proteins (see *Materials and Methods*). (**A**) *S. aureus* cells were treated with a dilution series of either AS or HIS, then probed with His-tagged forms of either CRIg-WT, CRIg-Mut-1, or CRIg-Mut-2. The fluorescence intensity observed in three technical replicates is plotted as a function of serum dilution, with a legend inset. (**B**) *S. aureus* cells were treated with 3% (v/v) of either AS or HIS, then probed with a dilution series of His-tagged forms of either CRIg-WT, CRIg-Mut-1, or CRIg-Mut-2. The fluorescence intensity observed in three technical replicates is plotted as a function of CRIg concentration, with a legend inset.

we proceeded to evaluate both PEG-modified forms of CRIg-Mut-1 in hemolysis experiments.

Due to the limited amounts of material available, we could not obtain full dose–response inhibition curves on both crosslinked forms of CRIg-Mut-1. Instead, we opted to investigate AP-mediated lysis of rabbit erythrocytes at three concentrations of unmodified CRIg-Mut-1 that gave suboptimal inhibition in our earlier experiment. We preincubated rabbit erythrocytes with CRIg-Mut-1, CRIg-Mut-1-PEG_{12}, or CRIg-Mut-1-PEG_{25} at 1.5, 3, and 6 μM protein (expressed in terms of the concentration of CRIg monomer present in each sample), added AS to activate the AP, and quantified the percent lysis spectrophotometrically following incubation at 37°C for a fixed interval (Fig. 5B). We found that unmodified CRIg-Mut-1 achieved mean values of 8.9, 24.5, and 58.6% inhibition of hemolysis at the concentrations used. In contrast, we found that CRIg-Mut-1-PEG_{12} showed mean values of 17, 32.2, and 76.1% inhibition of hemolysis at the same concentrations. This represents a statistically significant increase in inhibition ($p < 0.0001$) relative to unmodified CRIg-Mut-1 at all three concentrations tested. Curiously, we found that CRIg-Mut-1-PEG_{25} showed mean values of 8.9, 19.9, and 53% inhibition of hemolysis at these same concentrations. This represents a statistically significant loss in activity relative to the unmodified CRIg-Mut-1 control. Taken together, these observations reveal that crosslinked CRIg-Mut-1 can surpass the activity of the CRIg-Mut-1 protein alone, but they also suggest that the length of the crosslinker is critical to enhancing this complement-inhibitory activity.

DISCUSSION

CRIg belongs to a group of cell surface–exposed receptors that selectively bind to complement activation products and facilitate phagocytic uptake of complement-opsonized materials (7). In the absence of its transmembrane domain (Fig. 1A), however, the extracellular region of CRIg acts as complement inhibitor by virtue of its direct interactions with the C3 convertase component, C3b (7, 9, 11). CRIg shares some similarities to complement receptor 1 in this respect, which has been developed into a potent inhibitor of all three complement pathways, as it binds to both C4b and C3b (29). Because CRIg binds only to C3b and not to C4b as well (9, 11), it selectively inhibits the AP without any activity against the CP or LP. To capitalize on this useful property, Li et al. (18) used structure-based affinity maturation to identify increasingly potent variants of the CRIg C3b-binding domain (i.e., its N-terminal Ig V domain) on the premise that its intrinsic affinity for C3b was relatively weak (K_D = 1.1 μM). However, our results show that the affinity of CRIg-WT for C3b is significantly higher than previously reported, with values in the 10–100 nM range depending on the specific experimental conditions used (Fig. 3, Supplemental Figs. 2, 3, Table II). CRIg-Mut-1 and CRIg-Mut-2 likewise display C3b-binding affinities in this low-nanomolar range (Fig. 3, Table II). Although the reasons for the differences between our results and those reported

https://doi.org/10.4049/immunohorizons.2300064

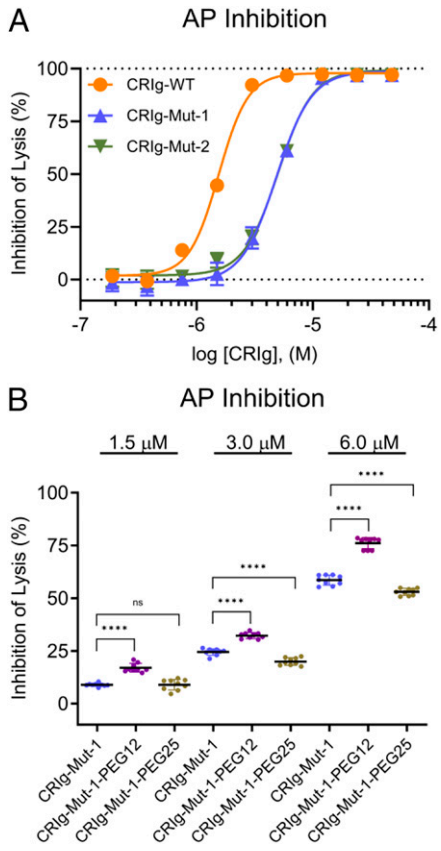

FIGURE 5. Inhibition of AP-driven hemolysis by lysine substitution CRIg mutants.

Rabbit erythrocytes were treated with 12% (v/v) AS either in the absence or presence of a dilution series of CRIg proteins. Hemolysis was assessed spectrophotometrically following a 30 min incubation at 37°C (see *Materials and Methods*). (**A**) Inhibition of hemolysis by CRIg-WT, CRIg-Mut-1, and CRIg-Mut-2, with a legend inset. Normalized values from three technical replicates are expressed as a function of CRIg protein concentration and were fit to a four-parameter dose–response curve. The IC_{50} values for each protein are as follows: CRIg-WT = 1.6 μM, CRIg-Mut-1 = 4.9 μM, and CRIg-Mut-2 = 5.0 μM. (**B**) Inhibition of hemolysis in the presence of 12% (v/v) AS by crosslinked CRIg-Mut-1-PEG_{12} and CRIg-Mut-1-PEG_{25} was compared with that of unmodified CRIg-Mut-1 as a control. Three different CRIg concentrations were used and nine technical replicates were performed. Each experimental group was compared with the corresponding unmodified control by an unpaired *t* test to assess statistical significance. ****$p < 0.0001$. ns, not significant.

previously are not certain, the use of Fc fusion proteins of CRIg and/or dimers of C3b in earlier binding studies could have been a factor (9). Because our experiments relied on soluble, monomeric forms of CRIg and C3b to obtain binding information, we propose that the affinity of CRIg for C3b is at least an order of magnitude tighter than initially believed.

We also found that all three forms of CRIg examined in this study displayed progressively weaker binding to downstream C3 activation products, particularly C3c (Table II). Indeed, the observed affinity of CRIg-WT and both mutants for C3c is between ∼10- and 100-fold weaker than what we measured for C3b and iC3b (Fig. 3, Supplemental Figs. 2, 3, Table II). These observations stand in contrast to earlier reports, which suggested that CRIg binds with comparable affinity to C3b and C3c (11). The differences in affinity we observed correlate with minor structural changes in the CRIg-binding site that occur as C3b is processed to iC3b and then C3c; however, according to the EBI-PISA server (30), there is ∼200 $Å^2$ more buried surface area at the CRIg/C3b interface when compared with that of CRIg/C3c. These changes are delocalized in nature, which might be expected given the discontinuous CRIg binding site on these C3 fragments (11). Because the proteolytic cleavages that mark the transition from C3b to iC3b to C3c happen at some distance from the CRIg-binding site itself (7), we suspect that changes in protein dynamics might occur upon cleavage that affect the CRIg-binding site in C3b/iC3b/C3c. From a biological standpoint, however, the differences in affinity of CRIg for C3c relative to C3b and iC3b could also serve a functional purpose: because C3c does not remain surface associated and has no known biological activity, having a lower affinity for this decoy ligand would make CRIg binding less likely while simultaneously favoring its interactions with the C3b and iC3b that remain covalently bound to complement-opsonized cells and materials. Thus, we suspect that this differential affinity for C3 fragments is an important feature to proper functioning of CRIg as a complement receptor that has been overlooked until now.

Although the ability of CRIg to selectively inhibit the AP makes it a promising candidate for therapeutic development, information presented in earlier publications suggested that the C3b-binding affinity of CRIg was too weak to be used for this purpose (11, 18). In fact, this was the very reason Li et al. (18) pursued a structure-based affinity maturation strategy to generate CRIg variants of increased affinity for C3b. Because multivalent molecules often exhibit enhanced functional properties through avidity effects, we sought to modify CRIg using an amine-reactive crosslinking approach. This required generating forms of CRIg that had minimal lysine content, which we thought was feasible because the structures of CRIg bound to C3b and C3c showed that its endogenous lysines play a minimal role in these protein–protein interactions (11). The two CRIg mutants we characterized in this study are essentially indistinguishable from CRIg-WT at the structural level (Figs. 1, 2). Although they show a mild ∼2- to 3-fold loss of activity in various functional assays (Figs. 3, 5A), they still bind C3b and iC3b in vitro and on cells and inhibit the AP-driven lysis of erythrocytes. Most importantly, we found that a crosslinked CRIg-Mut-1 dimer prepared using a bifunctional PEG_{12}-NHS ester displayed a significant increase in AP inhibition across a range of concentrations when compared with the unmodified protein (Fig. 5B). It is worth noting that although CRIg-Mut-1 contains only a single lysine residue (Fig. 1A), its N terminus also contributes a primary amine functional group; because of this, it is possible that the crosslinked dimers we prepared are a mixture of three different species. In the future, it may be worthwhile to evaluate a CRIg mutant that has no lysines

such that any amine-based crosslinking reactions would be restricted to the N terminus alone. Nevertheless, it is also interesting to consider preparation of other types of crosslinked species, such as those arising through use of activated dendrimers (31). Given the polyvalency possible through such approaches, we think that CRIg-modified dendrimers could exhibit quite potent AP inhibitory properties.

Another interesting outcome of our crosslinking study is that modification of CRIg-Mut-1 with PEG_{25}-NHS yields a product that is slightly, but significantly less active than the CRIg-Mut-1 alone (Fig. 5B). This result was unexpected, as we predicted that the longer length crosslinker would provide greater physical freedom for the modified CRIg-Mut-1 to bind C3b and thereby inhibit the AP. However, this appears not to have been the case. Although characterization of the CRIg-Mut-1-PEG_{25} adduct shows some evidence of chemical heterogeneity (Fig. 2A), we suspect that its diminished activity more likely results from physical incompatibility with C3b-containing species at the erythrocyte surface. Complement-mediated lysis of erythrocytes requires formation of the TCC, which requires cleavage of C5 by C3b-containing C5 convertases (1, 2). Because the AP C5 convertase (i.e., C3b3bBb) contains two copies of C3b yet becomes a progressively more efficient enzyme upon greater surface densities of C3b (4, 5), it is possible that CRIg-Mut-1 modified by an overly long crosslinker might not bind the convertase in an ideal orientation to inhibit C5 activation. Whereas a shorter length crosslinker may favor binding both copies of C3b within the same C5 convertase, a longer length crosslinker could promote binding between adjacent convertases or even other C3b molecules deposited on the surface, reducing the apparent inhibitory potency. Much remains to be learned insofar as the structure and function of C5 convertases are concerned. Consequently, we think that CRIg mutants crosslinked by PEGs of various lengths could be useful experimental tools for uncovering new structure/function information on C5 convertases. Considering the importance of these enzymes as therapeutic targets, we believe a continuation of these studies may be warranted.

DISCLOSURES

The authors have no financial conflicts of interest.

ACKNOWLEDGMENTS

X-ray diffraction data were collected at Southeast Regional Collaborative Access Team (SER-CAT) 22-ID beamline at the Advanced Photon Source, Argonne National Laboratory. A list of supporting institutions may be found on the SER-CAT Web site.

REFERENCES

1. Ricklin, D., G. Hajishengallis, K. Yang, and J. D. Lambris. 2010. Complement: a key system for immune surveillance and homeostasis. *Nat. Immunol.* 11: 785–797.
2. Hajishengallis, G., E. S. Reis, D. C. Mastellos, D. Ricklin, and J. D. Lambris. 2017. Novel mechanisms and functions of complement. *Nat. Immunol.* 18: 1288–1298.
3. Rawal, N., and M. K. Pangburn. 1998. C5 convertase of the alternative pathway of complement. Kinetic analysis of the free and surface-bound forms of the enzyme. *J. Biol. Chem.* 273: 16828–16835.
4. Rawal, N., and M. K. Pangburn. 2000. Functional role of the noncatalytic subunit of complement C5 convertase. *J. Immunol.* 164: 1379–1385.
5. Rawal, N., and M. Pangburn. 2001. Formation of high-affinity C5 convertases of the alternative pathway of complement. *J. Immunol.* 166: 2635–2642.
6. Rawal, N., and M. K. Pangburn. 2003. Formation of high affinity C5 convertase of the classical pathway of complement. *J. Biol. Chem.* 278: 38476–38483.
7. Geisbrecht, B. V., J. D. Lambris, and P. Gros. 2022. Complement component C3: a structural perspective and potential therapeutic implications. *Semin. Immunol.* 59: 101627.
8. Nauseef, W. M. 2007. How human neutrophils kill and degrade microbes: an integrated view. *Immunol. Rev.* 219: 88–102.
9. Helmy, K. Y., K. J. Katschke, Jr., N. N. Gorgani, N. M. Kljavin, J. M. Elliott, L. Diehl, S. J. Scales, N. Ghilardi, and M. van Lookeren Campagne. 2006. CRIg: a macrophage complement receptor required for phagocytosis of circulating pathogens. *Cell* 124: 915–927.
10. Gorgani, N. N., J. Q. He, K. J. Katschke, Jr., K. Y. Helmy, H. Xi, M. Steffek, P. E. Hass, and M. van Lookeren Campagne. 2008. Complement receptor of the Ig superfamily enhances complement-mediated phagocytosis in a subpopulation of tissue resident macrophages. *J. Immunol.* 181: 7902–7908.
11. Wiesmann, C., K. J. Katschke, J. Yin, K. Y. Helmy, M. Steffek, W. J. Fairbrother, S. A. McCallum, L. Embuscado, L. DeForge, P. E. Hass, and M. van Lookeren Campagne. 2006. Structure of C3b in complex with CRIg gives insights into regulation of complement activation. *Nature* 444: 217–220.
12. Forneris, F., J. Wu, X. Xue, D. Ricklin, Z. Lin, G. Sfyroera, A. Tzekou, E. Volokhina, J. C. Granneman, R. Hauhart, et al. 2016. Regulators of complement activity mediate inhibitory mechanisms through a common C3b-binding mode. *EMBO J.* 35: 1133–1149.
13. Morgan, B. P., and C. L. Harris. 2015. Complement, a target for therapy in inflammatory and degenerative diseases. *Nat. Rev. Drug Discov.* 14: 857–877.
14. Mastellos, D. C., D. Ricklin, and J. D. Lambris. 2019. Clinical promise of next-generation complement therapeutics. *Nat. Rev. Drug Discov.* 18: 707–729.
15. Rother, R. P., S. A. Rollins, C. F. Mojcik, R. A. Brodsky, and L. Bell. 2007. Discovery and development of the complement inhibitor eculizumab for the treatment of paroxysmal nocturnal hemoglobinuria. [Published erratum appears in 2007 *Nat. Biotechnol.* 25: 1488.] *Nat. Biotechnol.* 25: 1256–1264 .
16. Schatz-Jakobsen, J. A., Y. Zhang, K. Johnson, A. Neill, D. Sheridan, and G. R. Andersen. 2016. Structural basis for eculizumab-mediated inhibition of the complement terminal pathway. *J. Immunol.* 197: 337–344.
17. Katschke, K. J., Jr., K. Y. Helmy, M. Steffek, H. Xi, J. Yin, W. P. Lee, P. Gribling, K. H. Barck, R. A. Carano, R. E. Taylor, et al. 2007. A novel inhibitor of the alternative pathway of complement reverses inflammation and bone destruction in experimental arthritis. *J. Exp. Med.* 204: 1319–1325.
18. Li, B., H. Xi, L. Diehl, W. P. Lee, L. Sturgeon, J. Chinn, L. Deforge, R. F. Kelley, C. Wiesmann, M. van Lookeren Campagne, and S. S. Sidhu. 2009. Improving therapeutic efficacy of a complement receptor by structure-based affinity maturation. *J. Biol. Chem.* 284: 35605–35611.
19. Geisbrecht, B. V., S. Bouyain, and M. Pop. 2006. An optimized system for expression and purification of secreted bacterial proteins. *Protein Expr. Purif.* 46: 23–32.
20. Zhang, Y., A. J. Vontz, E. M. Kallenberger, X. Xu, N. T. Ploscariu, K. X. Ramyar, B. L. Garcia, B. Ghebrehiwet, and B. V. Geisbrecht.

2022. gC1qR/C1qBP/HABP-1: structural analysis of the trimeric core region, interactions with a novel panel of monoclonal antibodies, and their influence on binding to FXII. *Front. Immunol.* 13: 887742.
21. Otwinowski, Z., and W. Minor. 1997. Processing of x-ray diffraction data collected in oscillation mode. *Methods Enzymol.* 276: 307–326.
22. McCoy, A. J., R. W. Grosse-Kunstleve, P. D. Adams, M. D. Winn, L. C. Storoni, and R. J. Read. 2007. Phaser crystallographic software. *J. Appl. Cryst.* 40: 658–674.
23. Zwart, P. H., P. V. Afonine, R. W. Grosse-Kunstleve, L. W. Hung, T. R. Ioerger, A. J. McCoy, E. McKee, N. W. Moriarty, R. J. Read, J. C. Sacchettini, et al. 2008. Automated structure solution with the PHENIX suite. *Methods Mol. Biol.* 426: 419–435.
24. Adams, P. D., P. V. Afonine, G. Bunkóczi, V. B. Chen, I. W. Davis, N. Echols, J. J. Headd, L. W. Hung, G. J. Kapral, R. W. Grosse-Kunstleve, et al. 2010. PHENIX: a comprehensive Python-based system for macromolecular structure solution. *Acta Crystallogr. D Biol. Crystallogr.* 66: 213–221.
25. Boero, E., I. Brinkman, T. Juliet, E. van Yperen, J. A. G. van Strijp, S. H. M. Rooijakkers, and K. P. M. van Kessel. 2021. Use of flow cytometry to evaluate phagocytosis of *Staphylococcus aureus* by human neutrophils. *Front. Immunol.* 12: 635825.
26. Janssen, B. J. C., A. Christodoulidou, A. McCarthy, J. D. Lambris, and P. Gros. 2006. Structure of C3b reveals conformational changes that underlie complement activity. *Nature* 444: 213–216.
27. Jensen, R. K., G. Bajic, M. Sen, T. A. Springer, T. Vorup-Jensen, and G. R. Andersen. 2021. Complement receptor 3 forms a compact high-affinity complex with iC3b. *J. Immunol.* 206: 3032–3042.
28. Janssen, B. J. C., E. G. Huizinga, H. C. A. Raaijmakers, A. Roos, M. R. Daha, K. Nilsson-Ekdahl, B. Nilsson, and P. Gros. 2005. Structures of complement component C3 provide insights into the function and evolution of immunity. *Nature* 437: 505–511.
29. Krych-Goldberg, M., and J. P. Atkinson. 2001. Structure-function relationships of complement receptor type 1. *Immunol. Rev.* 180: 112–122.
30. Krissinel, E., and K. Henrick. 2007. Inference of macromolecular assemblies from crystalline state. *J. Mol. Biol.* 372: 774–797.
31. Abbasi, E., S. F. Aval, A. Akbarzadeh, M. Milani, H. T. Nasrabadi, S. W. Joo, Y. Hanifehpour, K. Nejati-Koshki, and R. Pashaei-Asl. 2014. Dendrimers: synthesis, applications, and properties. *Nanoscale Res. Lett.* 9: 247.